POLITECNICO DI TORINO
Repository ISTITUZIONALE

Use of electrode displacement signals for electrode degradation assessment in resistance spot welding

(Article begins on next page)

08 November 2022

Use of Electrode Displacement Signals for Electrode Degradation Assessment in Resistance Spot Welding

∗**Luigi Panza**[1][0000-0003-1461-3337]**, Manuela De Maddis**[1][0000-0002-2459-2501]**, Pasquale Russo Spena**[1][0000-0003-0307-2344]

[1] Department of Management and Production Engineering, Politecnico di Torino, Turin 10129, Italy
e-mails: luigi.panza@polito.it, manuela.demaddis@polito.it, pasquale.russospena@polito.it
* Corresponding author

Abstract

In resistance spot welding, the quality of welds is not only affected by the correct design of the welding cycle, but also by the electrode degradation that occurs over time. This work proposes a novel approach to indirectly monitor the electrode degradation during welding by analyzing the electrode displacement signal from a non-contact sensor embedded in the welding machine and the electrode tip shape obtained from carbon imprint tests. As a result of an experimental campaign involving more than 1200 weld spots, the electrode speed during the final hold stage has been determined as the most explanatory feature describing the electrode displacement. Based on the mechanical strength of spot welds, the electrode contact face area has been defined as the most representative feature characterizing electrode degradation. A regression analysis has been carried out to infer a relationship between the electrode speed and the contact area representative of tool wear. A Neural Network has been built to use some features extracted from the electrode displacement signals to predict the contact area and thus indirectly the electrode degradation.

Keywords: Resistance Spot Welding, Electrode Degradation, Electrode Displacement, Wear Monitoring, Neural Network

1. Introduction

Resistance Spot Welding (RSW) is a joining technique commonly used in many industrial fields because of its easiness, automatability, and low production costs [1]. Although these advantages, the assessment of the quality of spot welds poses some issues because of the complexity of the joining process and the presence of several interacting factors, including the chemical composition of the sheet stack, electrode wear, machine compliance, and so forth. Moreover, the non-direct visibility of the joint, because the weld nugget remains inside the sheet stack, makes necessary time-consuming experimental campaigns and destructive tests to evaluate joint quality, with an economic loss for companies [2]. Therefore, considerable attention has been devoted to monitoring the welding process to gain information contained in the welding signals (e.g., welding voltage and power, electrode displacement, dynamic resistance of the sheet stack) to control the process, ensure quality welds, or predict in real-time nugget size and mechanical strength of spot welds.

Zhao et al. [3] used some features extracted from the electric power signal to feed a Neural Network (NN) and predict the nugget size of spot welds. X. Wan et al. [4] built a NN based on the features extracted from voltage signal to predict different quality levels (e.g., weld strength and nugget size) of spot welds. The same authors [5] also used a NN to predict both the nugget dimension and the mechanical strength of spot welds based on some features extracted from the electrical resistance signal. Other works have also been conducted for weld quality prediction [6] [7] by analyzing the electrode displacement during welding. Y.S. Zhang et al. [8] used a neuro-fuzzy system to manage the welding current to balance the electrode wear and, hence, keep a constant joint quality (i.e., similar nugget size and mechanical strength) over time. Xia et al. [9] found a clear relationship between the abrupt change of electrode displacement during the welding expulsion and the corresponding amount of expelled material. L. Zhou et al. [10] have employed two different adaptive control strategies by using respectively the electrode displacement signal and the dynamic resistance signal with the aim to monitor the process in non optimal welding conditions. When the weld spot was carried out close to the sheets edge, as well as when there was a gap between the sheets to be welded, the control strategy by means of electrode displacement signals outperformed the one with the dynamic resistance signal of the sheet stack. Zhao et al. [11] employed process signals to obtain the optimal values of several welding quality indexes, such as the nugget dimension, mechanical strength, electrode displacement peak, and stored energy in the joint before to reach the failure.

All these works have assessed the spot weld quality regardless of electrode degradation. This phenomenon can be neglected for experimental tests where a limited number of spots are realized with unused electrodes, whereas it assumes notable importance on spot weld quality when electrodes are used hundreds of times, as it occurs in industrial production. In this case, electrodes are subjected to complex and different damage mechanisms, such as plastic deformation, pitting, creep, and thermal fatigue [12], because of the collective effects of elevated temperature, high mechanical pressure, and atomic diffusion between electrodes and sheets [13]. This leads to the degradation of electrodes with different macroscopic evidence. On one hand, the irreversible deformation of the electrode tips causes an increase of the face areas, which reduces current density. As a result, welding using a current value as designated when the electrodes were new will lead to substandard spots due to insufficient current density. On the other hand, electrode wear yields an irregular electric current distribution through the sheet stack that contributes to a worsening of the joint quality and reduces the repeatability of weld performances. For these reasons, electrode tip diameter and contact area are commonly accepted as parameters characterizing the electrode degradation [14]. Many works have focused attention on the electrode wear effect on weld quality, but often with a lack of accurate methodologies for a quantitative prediction of electrode degradation. Some authors have proposed some approaches to monitor the electrode deterioration through the analysis of the welding signals, including welding current, dynamic resistance, electrode displacement. L. Zhou et al. [15] exploited the similarity techniques among several electrical resistance curves over time for the detection of electrode deterioration. The evolution of the dynamic resistance signal over time has been associated with the different electrode wear stages by establishing a qualitative technique for the online monitoring of electrode degradation. Y.S. Zhang [16] used Statistical Process Control techniques applied to the electrode displacement signal for monitoring the stability of the RSW process during the electrode deterioration. Based on the variation of the electrode displacement curves, they also set a Neuro-Fuzzy control of the welding current to compensate for the electrode wear on weld

strength and nugget size. A similar monitoring technique was also used by [17] in which a moving range chart was used to indirectly assess the electrode wear through the information contained in the electrode displacement signal.

In an industrial context, the assessment of the electrode degradation relies on the human operator experience or qualitative estimates, without employing quantitative methodologies. The lack of a real-time and objective system able to relate the electrode degradation to joint quality leads to having in a car body approximately 1000-1200 spot welds more than required to balance the possible presence of improper joints [15]. Therefore, research methodologies for the quantitative and accurate assessment of the electrode condition are of utmost importance to avoid unnecessary and improper weld spots. Moreover, they would allow to replace or dress electrodes just before the achievement of critical wear conditions, thereby saving resources, reducing costs, and having more reliable and repetitive high-quality spot welds. For such reasons, more efforts could be oriented towards the quantitative prediction of the electrode degradation during the RSW through the exploitation of sensor data gatherable during the welding process through Prognostic Health Management (PHM) activities [18].

This work aims to set a methodology to predict the electrode degradation based on the electrode displacement signal acquired during an experimental RSW campaign performed on DP590 steel sheets. The adopted approach consists of collecting the electrode displacement with an increasing number of spot welds through a non-contact sensor embedded in the welding machine. The most significant features characterizing the electrode displacement are extracted from the data acquired by the sensor. At the same time, the electrode degradation over time has been assessed through the measurement of geometrical characteristics of the electrode contact face as obtained by a carbon imprint test. Based on the mechanical strength of weld spots, the most important geometrical feature describing the electrode imprint has been chosen as an indicator of electrode degradation. A regression analysis has been carried out to infer a relationship between the electrode wear indicator and the most explanatory feature computed from the electrode displacement curve. As discussed thereafter, other features extracted from the electrode displacement signal have also been selected as input variables to feed a Neural Network to accurately predict the wear indicator and, in turn, for real-time monitoring of the electrode degradation through a Machine Learning algorithm.

2. Experimental Procedure

The experimental campaign has involved more than 1200 spot welds executed on DP590 galvanized steel sheets, commonly used to produce car body parts (e.g., wheel webs, lightweight sections, strut mounts, fasteners, etc.) in the automotive industry. The sheets were 1 mm thick.

The spot welds were obtained with an industrial medium frequency direct current (MFDC) resistance spot welding machine by Tecna, with a maximum welding power of 650 kVA. The machine was equipped with a fiber-optic position sensor to detect the electrode displacement during welding at a resolution of 2 μm. The RSW machine mounted two trucanted cone shape electrodes made of Cu-Cr-Zr alloy, with a contact nominal diameter of 6 mm (area 28.3 mm^2) according to the recommendations of the AWS D8.9 M standard (American Welding Society 2012). Detailed geometry of the electrodes is shown in Fig. 1. During welding, the electrodes were cooled by means of a water flow about 4 l/min. The bottom electrode was fixed, whereas the top electrode moved to clamp the sheet stack.
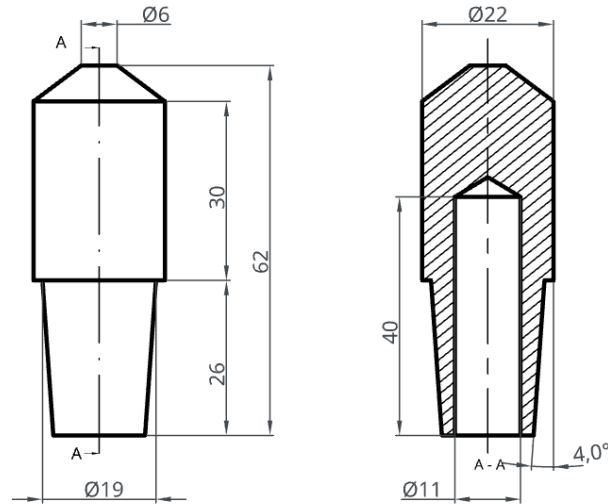
Fig. 1. Geometry of the truncated cone electrodes.

An endurance test based on AWS D9.8 M standard has been performed to investigate the electrode degradation. Hundreds of spot welds were consecutively realized using the same welding cycle until the full damage of the electrodes, which was based on the results of the shear tension tests. The spot weld cycle used in the RSW tests is schematically displayed in Fig. 2. Previous pilot experimentation had been carried out to define the process parameters.
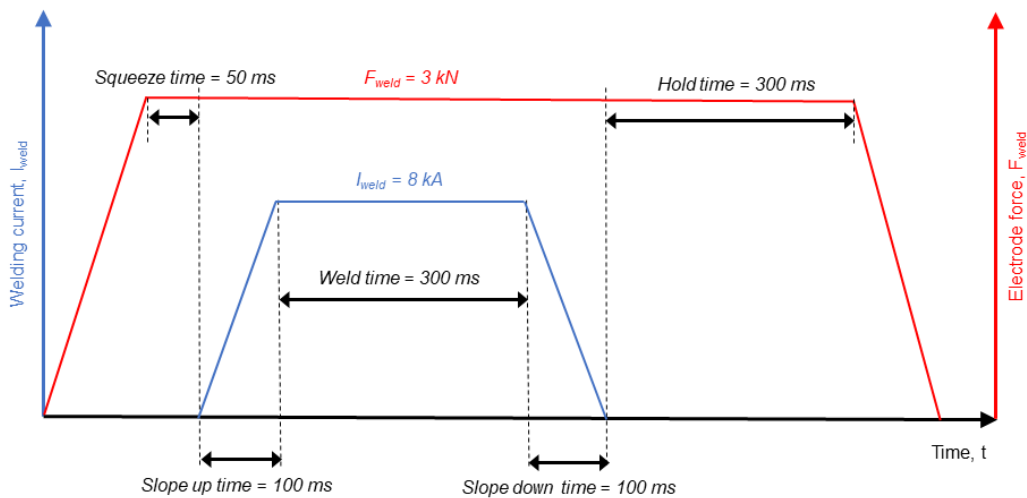
Fig 2. Schematization of the spot weld cycle used in the experimental campaign.

The endurance test was carried out by using 9 couples of overlapped sheets, namely panel weld, with a 300 mm x 200 mm size, Fig. 3. Each couple of sheets was spot welded along 9 rows of 15 points each. Overall, 1215 spots were welded. The specified edge and weld spacing distances and the execution sequence were maintained on all the panel welds.

4
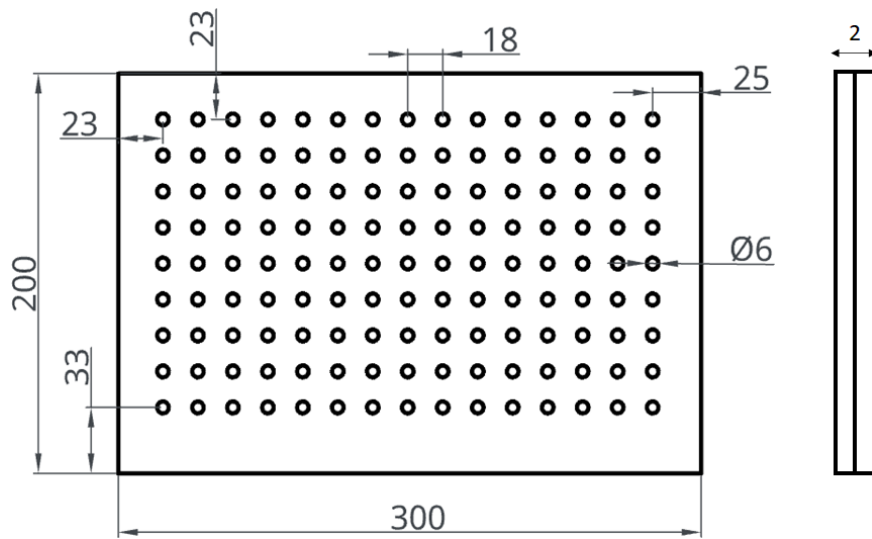
Fig. 3. Edge and weld spacing distances used on the panel welds for the endurance test according to the AWS D9.8 M standard.

Overall, the procedure adopted during the welding campaign is described in the following:

a) The initial contact area of the unused electrode tips was assessed through a carbon imprint test. In this test, a metal sheet wrapped in two paper layers was used. The outermost layer was made of black carbon paper, whereas the other one was blank paper. A complete welding cycle was executed without flowing the electric current. The electrode imprints left by the carbon papers on the white one were used as a measure of the damage of the electrode faces.

b) The zeroing of the electrode displacement signal was performed by closing with a little pressure, without the application of welding current, the electrodes against the sheet stack. The zero signal was defined when the electrode faces were in contact with the sheet surfaces.

c) The first spot weld was realized on the weld panel. After that, three successive spot welds were performed on overlapped strips to obtain three welded samples for the shear tension test. In this way, the mechanical strength of the weld spots obtained from unused electrodes could be determined.

d) Further spot welds were realized on the overlapped sheet for the endurance test. Whenever a row of 15 spot welds was executed (Fig. 3), the electrode degradation was measured through the carbon imprint test by the imprints left on blank paper. After that, the endurance test could continue. Whenever a couple of overlapped sheets was welded (135 welds), three welded samples were prepared for the shear tension test. Thus, the mechanical strength of spot welds could be detected at different stages of electrode degradation.

e) The above-mentioned procedures were repeated for each of the 9 pairs of welded panels.

The shear tension samples were 30 mm x 100 mm, with an overlapping area of 30 mm according to the JIS Z 3136 (Japanese Standards Association, 2018), Fig. 4. Shims on the sheets ends were used to avoid the bending of the weld panels during the experimentation. The shear tension tests were carried out with a crosshead speed of 10 mm/min by employing a standard testing machine. Shear tension strength has been evaluated as the maximum force reached during the test. The peak load has been considered as the parameter to evaluate the effect of electrode degradation on joint quality. The critical wear damage of electrode has been determined as soon as the strength of the spot welds reduced below a threshold value, identified as 80% of the initial peak load [14], [19].
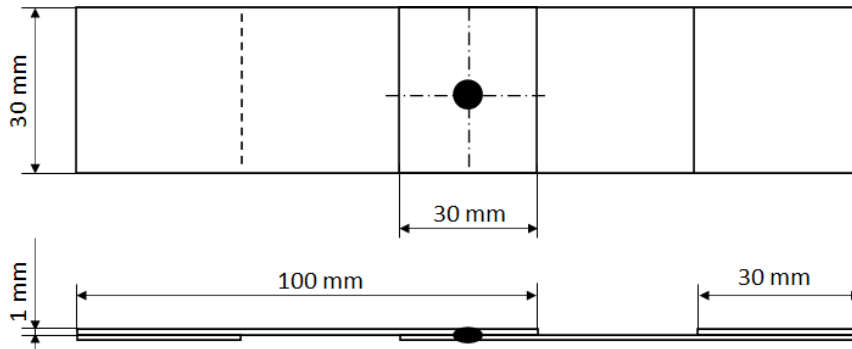
Fig. 4. Geometry of the shear tension samples according to JIS Z 3136 standard.

The displacement of the moving electrode has been acquired by the non-contact sensor for all the spot welds performed in the endurance test. The post-processing of the electrode imprints and electrode displacement signals, the statistical analysis, and the learning algorithm, based on a Neural Network, used to monitor and predict electrode degradation, are discussed in the following paragraphs.

3. Results and Data Analysis

3.1 Shear tension tests

The results of the shear tension tests are displayed in Fig. 5. Three colors (black, blu, and red) have been used to discriminate the weld spots with different mechanical properties as a function of the number of welds. The colored points have also been used in the figures that follow in the main text. Black dots highlight the region where the mechanical strength of the spot welds is always over the minimum shear strength value, 8 kN, and with repetitive values (0-800 range). Blue dots describe a transition zone where the weld spots start to show less repeatability with the occurrence of a noteworthy lowering of the weld strength (800-1000 range), with the occurrence of the first weld spot with shear strength lower than the minimum value. Finally, red dots mark an unstable welding process characterized by high variability of the strength values, often below the minimum shear strength. In this region, the electrode wear is such as to produce undersized welded nugget, often with local unwelded areas (1000-1245 range).
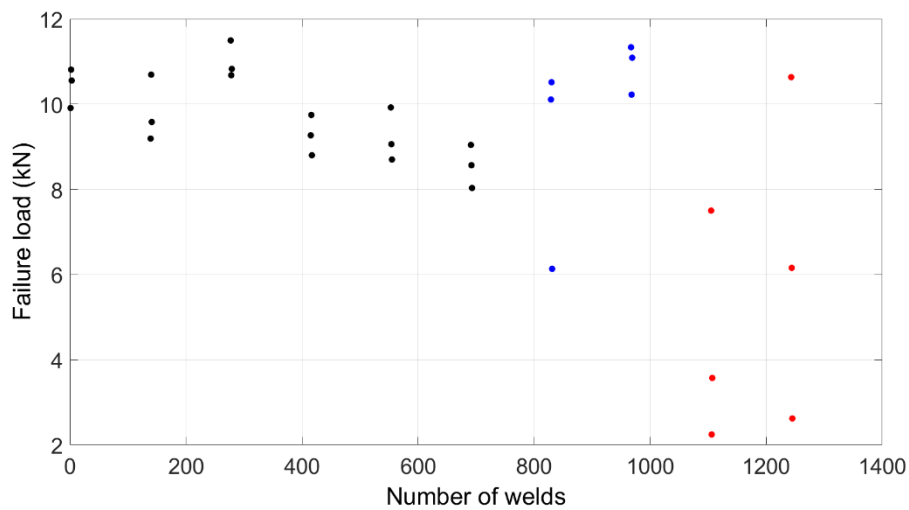

Fig. 5. Shear tension strength of the welded spots at varying number of welds.

The trend of the strength data is coherent with previous studies available in the literature that investigated the effect of electrode wear on the mechanical performance of spot welds [19], [20], [21].

3.2 Image processing

The geometrical features characterizing the electrode degradation have been extracted from the carbon imprint tests through image processing. Firstly, the electrode imprints were converted into image format using a scanner. As shown in Fig. 6, the carbon imprint test highlights the electrode degradation with an increase in the contact area (black area) due to the plastic deformation at high temperature, which also shortened the electrode length. Moreover, pitting damage (white zone) occurred firstly along the edges of the electrodes, and then in the central zone. MATLAB Image Processing Toolbox was employed to extract from the scanned images some geometrical features that could be considered as possible wear indicators characterizing the electrode degradation.
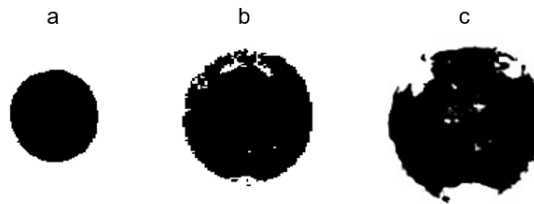

Fig. 6. Electrode tip shape as obtained from the carbon imprint tests at **a)** 0 welds, **b)** 600 welds, **c)** 1200 welds.

Although several geometrical characteristics have been computed from the imprint images, only those listed in the following can be related to the electrode deterioration process:

- *contact area:* number of pixels involved in the black region (contact zone) of the analyzed imprint;
- *equivalent diameter:* diameter of a circle with an area equal to the electrode contact area;
- *perimeter:* linear index of the pixels around the boundary of the imprint;
- *major contact length:* number of pixels of the major axis of the ellipse containing the imprint;
- *minor contact length:* number of pixels of the minor axis of the ellipse containing the imprint;
- *circularity factor:* electrode contact area divided by the area of a circle having the same perimeter.

With the purpose to select the most suitable indicator describing the electrode wear, the above geometrical features have been plotted as a function of the number of welds and failure load, as displayed by Fig. 7 and Fig. 8, respectively.
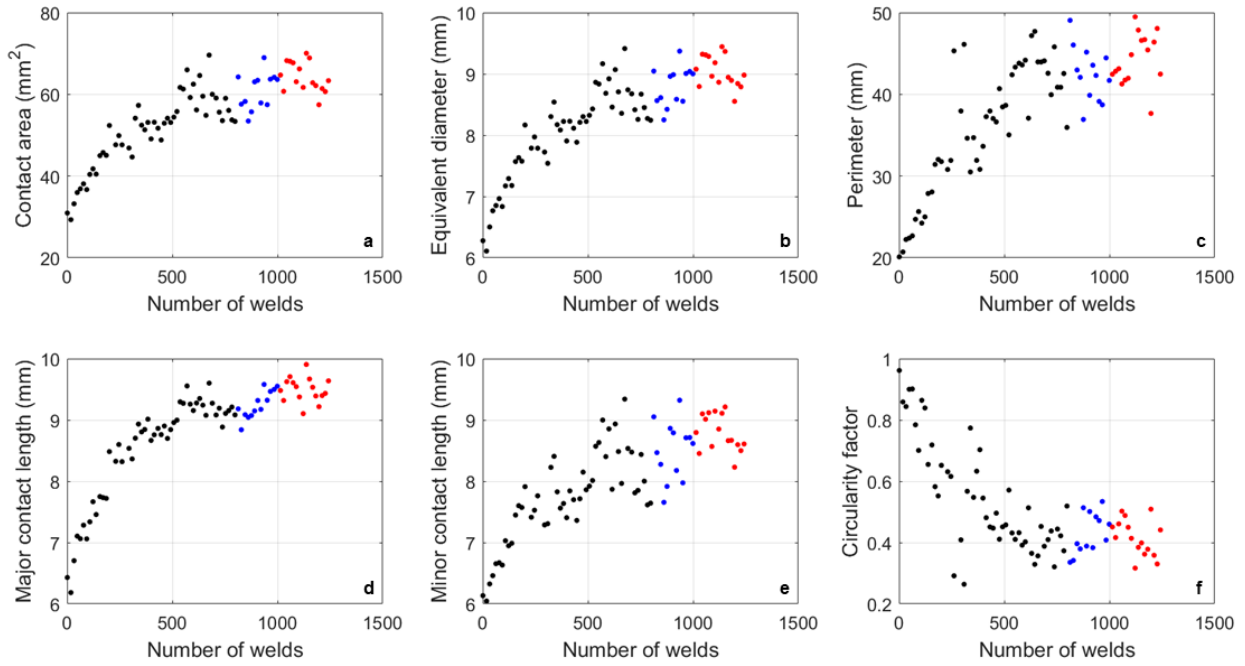
Fig. 7. Geometrical features extracted from the electrode carbon imprint vs. the number of welds.

All the geometrical features change continuously with the electrode degradation. The contact area increases over time because of the plastic deformation at elevated temperatures of the electrode face (Fig. 7a). Initially, the contact area increases with low variability and a steep rate, then, as the pitting zones formed and grew, the variability becomes larger whereas the rate reduces. The equivalent diameter has been directly computed by the contact area, so a similar behavior can be observed for this feature (Fig. 7b) and the major contact length (Fig. 7d). The perimeter and minor contact length of the electrode imprints show an overall increase, even if with a higher variability than the other geometrical features (Fig. 7c, Fig. 7e). The circularity factor constantly decreases until about 700 welds, and then it starts to show a variable trend (Fig. 7f).
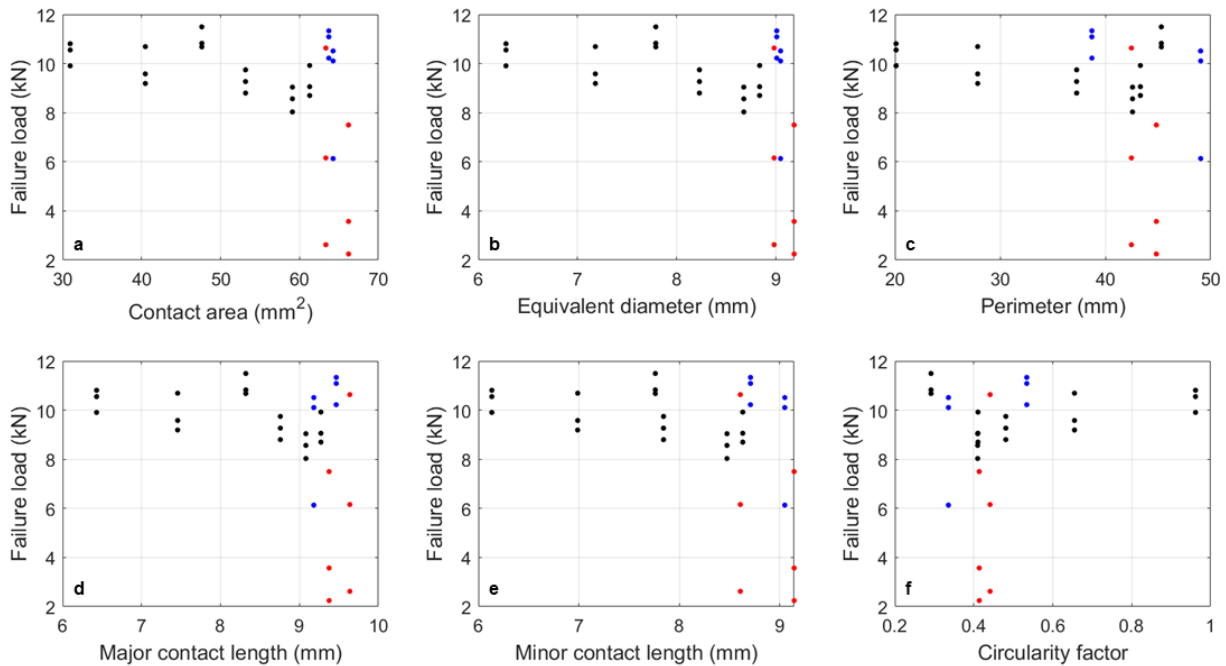

Fig. 8. Failure load of the welded joints vs. the electrode imprint features.

8

Fig. 8a displays the failure load of the spot welds as a function of the contact area. The mechanical strength values increase in variability when the contact area overcomes 62 mm^2 (2.2 times greater than the initial contact area) and, for some weld spots, it can be observed a drop of their mechanical strength. It should be noted a clear distinction of the black dots from the others as for the shear tension values displayed in Fig. 5. The same tendency is for the equivalent diameter, Fig. 8b, since it is directly computed from the contact area. The other geometrical characteristics extracted from the electrode imprints, as displayed in Fig. 8c to Fig. 8f, do not evidence a clear transition between sounds joints and improper spot welds, being black, blue, and red dots overlapped in some regions of the graphs. Based on such considerations, the contact area can be regarded to be the geometrical characteristic of the electrode imprint more capable to describe the influence of the electrode degradation on the joint strength. Therefore, the contact area has been chosen as the wear indicator to estimate electrode degradation. Since the electrode face cannot be measured continuously during a real industrial process, this geometrical feature has been evaluated through the electrode displacement signal measured during the welding process.
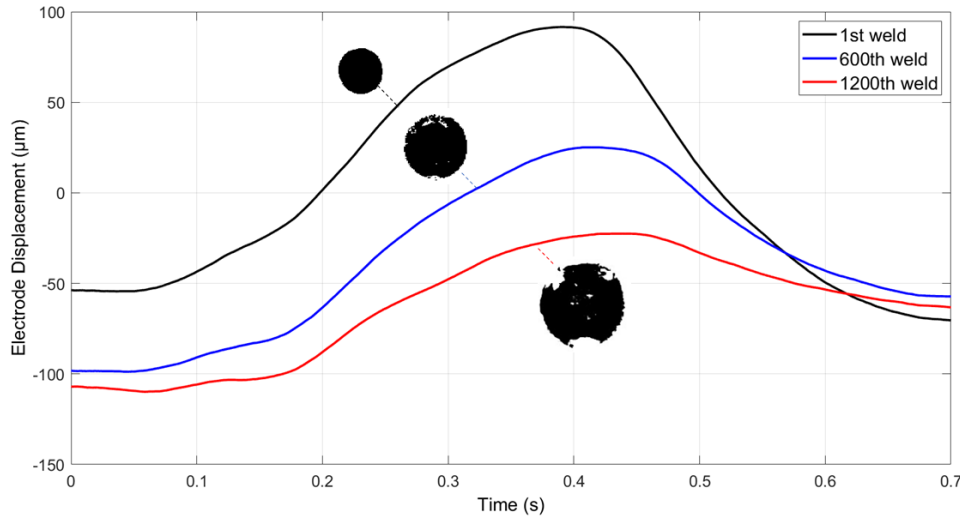
3.3 Electrode displacement processing

Fig. 9 displays a typical electrode displacement curve (Fig. 9a) from the beginning of the current passage to 200 ms after its shutdown (Fig. 9b). The electrode displacement signal is triggered by the welding current; therefore, the electrode signal is acquired as soon as the welding current starts to pass through the electrodes and the sheet stack. At that time, the electrodes are already pressed on the sheet stack because of the previous squeeze stage and, thus, the electrode displacement starts with a negative value. As the current rises, the region of the sheet stack crossed by the current increases in temperature and expands its volume. Such thermal expansion causes a lifting of the top electrode (i.e., the moving electrode) during the welding until it reaches a peak, which is related to the nugget size [22], [23]. Then, the temperature of the sheets reduces when the electric current drops, with a consequent volumetric contraction and reduction of the electrode displacement. It should be noted that the electrode displacement does not end up with the zeroing of the electric current because of the electrode indentation on the sheet surfaces.
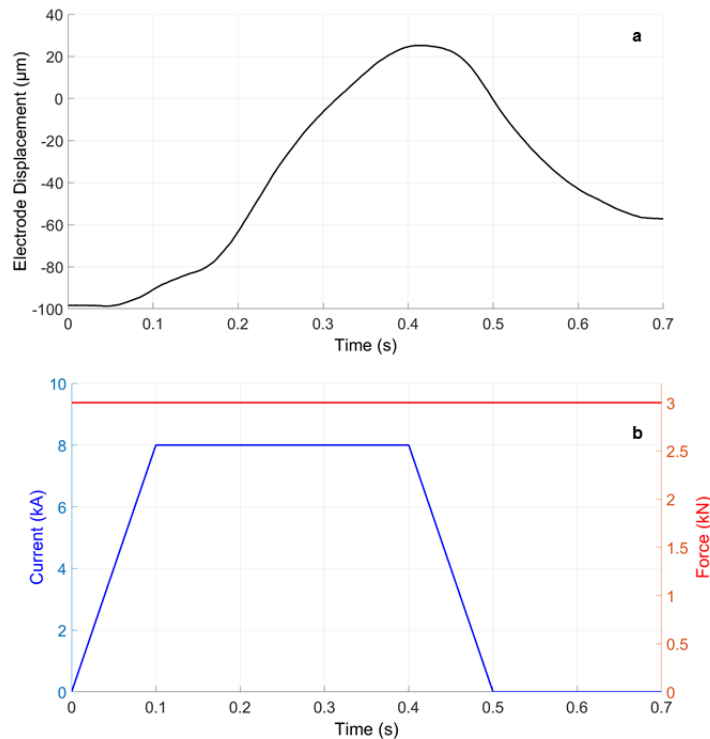
Fig. 9. A typical (a) electrode displacement curve with (b) the corresponding spot weld cycle.

Fig. 10 shows the electrode displacement curves obtained welding the 1st, 600th, and 1200th weld, and their relative electrode carbon imprint images.

Fig. 10. Different electrode displacement curves with associated electrode imprints.

As the deterioration process advances, the electrode requires a longer stroke to clamp the sheet stack because of the mushrooming of the electrode, caused by its plastic deformation, and wear. The initial electrode displacement moves from about -50 to -100 μm from the first spot weld to the 1200th, Fig. 10. The amplitude of the displacement curves decreases with the number of spot welds. The enlargement, wear, and oxidation of the contact face reduce the thermal power developed at the faying interface of the sheets. Consequently, it heats less, a lower amount of metal is melted, and, in turn, the welded joint expanded volumetrically less than it did at the beginning of the endurance test. Fig. 10 shows how the amplitude of the displacement curves, evaluated as the distance between the beginning and the peak value of the electrode displacement, moves from about 150 to 75 μm. For the same reason, the slope of the electrode displacement curve reduces, particularly in the final cooling (hold) stages.

Several statistics have been computed from the electrode displacement curve to extract the features to be related to the electrode condition indicator, that is the contact area. The correlation between the variables has been assessed using the Pearson coefficient as a measure of linear dependency. The inspected weld spots are those corresponding to the electrode wear measurements performed with the carbon imprint tests. All the statistics have been computed by considering a time range of 700 ms, from the turn on of the electric current until 200 ms after its switch off. Several features have been extracted from the electrode displacement curves and plotted as a function of the contact area. However, based on correlation coefficient values and graphical observations of the scatter plots, only the significant features have been selected, as follows:

- *maximum displacement:* peak value of the electrode displacement curve;
- *mean displacement:* average value of the electrode displacement curve;
- *standard deviation:* variability of the electrode displacement data around its mean;
- *Euclidean distance from the 1st weld:* square root of the sum of squared differences between the data obtained from the first electrode displacement curve and the following curves. It is a measure of how the displacement curve changes with the electrode degradation as compared to that obtained from unused electrodes;

10

- *average decreasing slope during the hold time stage:* assessed in the first 100 ms of the hold time stage as $(D_{600ms} - D_{500ms})/100$ ms, where D_{600ms} is the displacement value at 600 ms, D_{500ms} the displacement value at 500 ms, and 100 ms the time interval.
- *skewness:* asymmetry of electrode displacement data around its mean.

The evolution of such features over the number of welds is displayed in Fig.11.
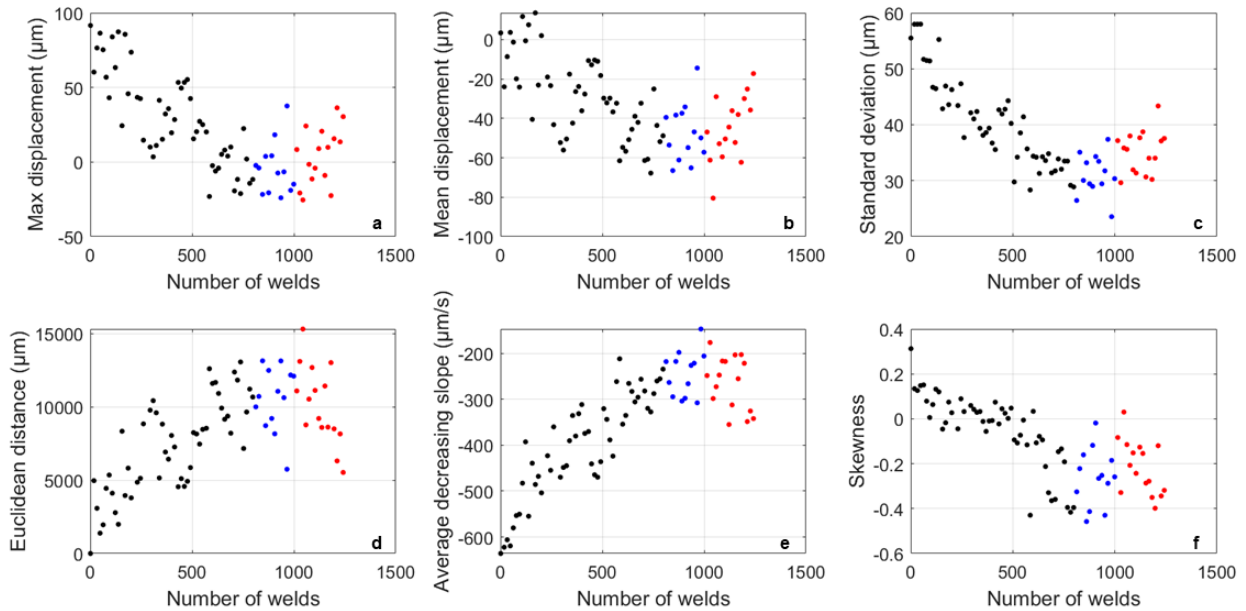
Fig. 11. Geometrical features extracted from the electrode displacement curve vs. the number of welds.

As previously discussed, the maximum displacement continuously falls with the electrode degradation because of the reduction of thermal power at the faying surface. It varies quite randomly when the electrode reaches its critical condition after 800 welds due to the process instability (Fig. 11a). Similar behavior occurs for the mean displacement and standard deviation, displayed respectively in Fig. 11b and Fig. 11c. The former has a trend more variable because it averages all the values of the displacement curve, and, thus, includes several phenomena (i.e., the different initial values, the different peak values, the different slope ups and slope downs, and so forth). The standard deviation is more related to the thermal power density because it measures the variability of the displacement values from its average value. For this reason, it shows a clearer trend with the number of welds. As expected, the Euclidean distance increases with the electrode degradation, even if with high variability (Fig. 11d). During the hold stage, the movement of the electrode becomes slower (Fig. 11e) coherently with the minor volumetric change occurring in the weld region because of the less thermal input available for the formation of the joint. The different initial values of the electrode displacement curve and the slower electrode displacements lead to a decreasing value of the skewness over the number of welds, as depicted in Fig. 11f.

Fig. 12 displays the scatter plots about the selected features of the electrode displacement signal and the contact area extracted from the electrode imprints, as well as the Pearson correlation coefficient, for each pair of variables.
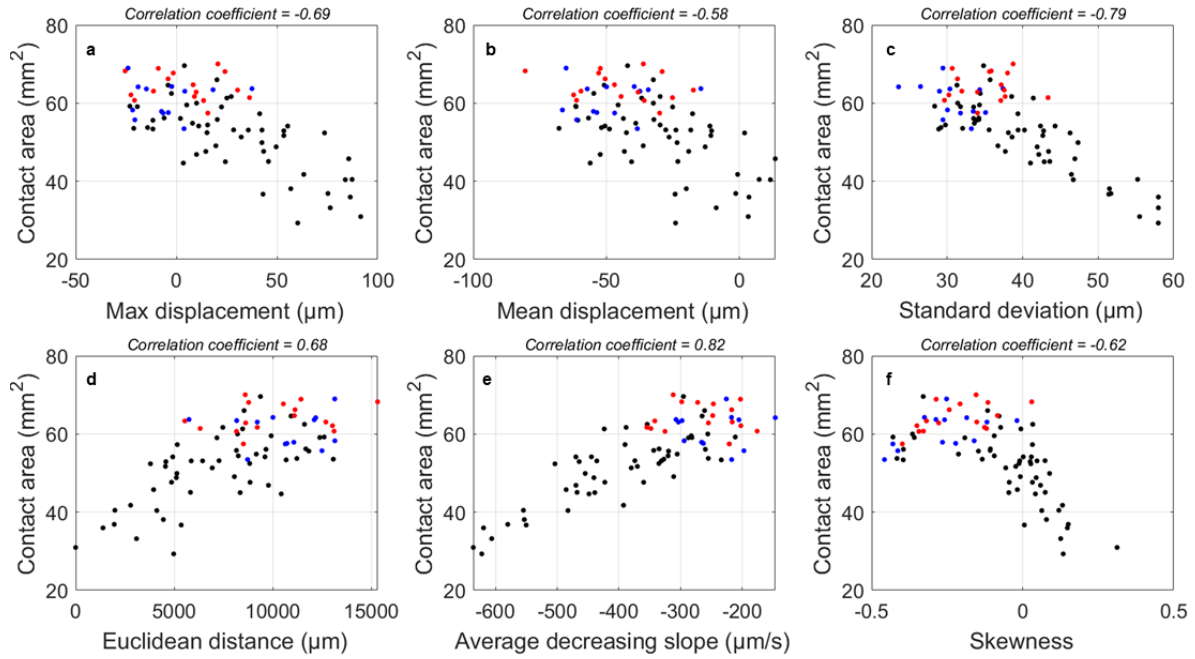
Fig. 12. Scatter plots of the electrode wear indicator, i.e., the contact area, vs. the predictive variables.

The scatter plots displayed in Fig. 12 confirm the relationship between the selected features extracted from the electrode displacement and the contact area. An increase in the contact area leads to a reduction of the maximum displacement and standard deviation. Conversely, the distance between the electrode displacement curves and the initial one increases, as shown by the scatter plot of the Euclidean distance in Fig. 12d. Both the average decreasing slope and the skewness show a clear relationship with the contact area. The standard deviation and the average decreasing slope are the electrode displacement features most correlated with the contact area, with a Pearson correlation coefficient of - 0.79 and 0.82, respectively. A statistical framework based on a regression analysis has been used to infer a relationship between the electrode wear indicator (i.e., contact area) and the electrode displacement curve. Moreover, a Machine Learning algorithm has been built to predict accurately the evolution of electrode contact area with the number of spot welds, based on some features extracted from the electrode displacement curve.

3.4 Inferential analysis

The purpose of the inferential analysis is to find an accurate mathematical model that can explain the relationship between predictive variables and a response variable. In this work, the candidate predictive variables are the statistical indexes extracted from the electrode displacement curve discussed in the previous paragraph, while the response variable is the contact area extracted from the electrode imprint images. From an inferential standpoint, the multicollinearity problem among predictors is an important issue; indeed, in the case of dependency among predictors, the explanation of the response variable would be assigned incorrectly to predictors. An adequate technique to address this issue is to define a correlation matrix involving the correlation coefficient computed for each pair of predictors to detect linear dependency on one another. Table 1 displays the correlation matrix with the predictive and response variables obtained from the welding tests.

Table 1
Correlation matrix between the predictive and response variables obtained from the welding experiments.

	Contact area	Max displacement	Mean displacement	Standard deviation	Euclidean distance	Decreasing slope	Skewness
Contact area	1	-0.69	-0.58	-0.79	0.68	**0.82**	-0.62
Max displacement	-0.69	1	0.96	0.88	-0.97	-0.85	0.71
Mean displacement	-0.58	0.96	1	0.73	-0.97	-0.70	0.54
Standard deviation	-0.79	0.88	0.73	1	-0.83	-0.94	0.76
Euclidean distance	0.68	-0.97	-0.97	-0.83	1	0.80	-0.63
Decreasing slope	**0.82**	-0.85	-0.70	-0.94	0.80	1	-0.82
Skewness	-0.62	0.71	0.54	0.76	-0.63	-0.82	1

The correlation analysis shows how the predictive variables are highly correlated with one another. Therefore, they cannot be considered independent, which is one of the key assumptions of linear regression. The correlation matrix shows that the average decreasing slope is the predictive variable that better explains the contact area variation during the electrode deterioration process. This predictive variable has been normalized with the standardization technique to rescale data in a proper range. Then, a 2nd-degree polynomial function has been defined as a regression model:

$$Y = b_o + b_1 x_1 + b_2 x_1^2 + \varepsilon \qquad (1)$$

where Y is the contact area, x_1 is the normalized average of the decreasing slope of the electrode, b_0, b_1, and b_2 are the coefficient estimates of the model, and ε is the residual between the observed value and the predicted one. The coefficient estimates of the regression model are reported in Table 2.

Table 2
Coefficient estimates of the regression model of Eq. 1.

Coefficient	p-value	Estimate	95 % Confidence interval
b_0	<0.00001	57.03	[55.49, 58.56]
b_1	<0.00001	6.58	[5.23, 7.94]
b_2	0.00061	-1.86	[-2.90, -0.82]

The coefficient estimates show a low p-value, that is they are highly statistically significant in the explanation of the response variable. Moreover, the 95 % confidence intervals are quite narrow. The polynomial regression model is plotted in Fig. 13. The coefficient of determination R^2 is 0.72, hence, the decreasing electrode speed after the current switch off can almost explain 3/4 of the total variation of the contact area during the electrode degradation process. This can be considered quite satisfactory to explain the electrode degradation through a single process signal. As RSW involves different physical phenomena, such as mechanical, electrical, thermal, and metallurgical mechanisms, more insights about the electrode degradation process could be gained through multi-fusion sensor techniques using welding signals, including electrical power, electrode voltages, and dynamic resistance, as suggested by [24] and [25]. In this way, a higher coefficient of determination R^2 could be achieved to explain the contact area variation during the electrode deterioration process.
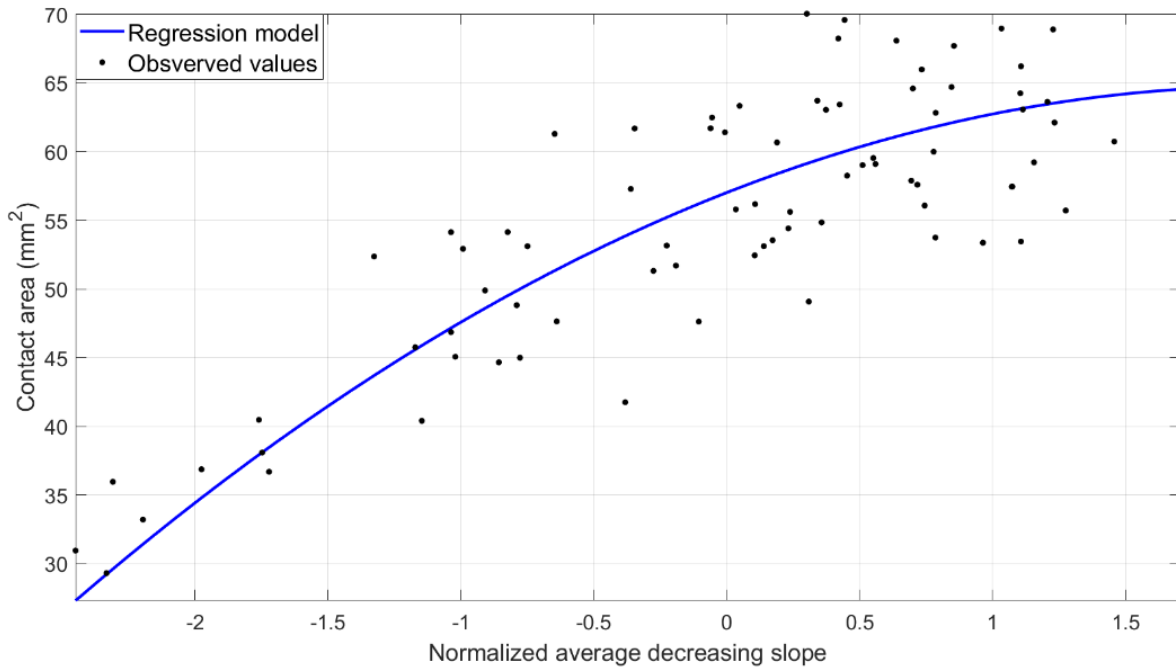
Fig. 13. Fitting of the contact area vs. normalized decreasing speed with the polynomial regression model.

Fig. 14 displays the graphical residual analysis needed to check whether the preliminary assumptions about the linear regression are satisfied or not. In particular, the normal distribution of residuals and homoscedasticity are required. Fig. 14a shows the residuals over the number of observations, while Fig. 14b shows the residuals over the fitted values by the regression model. Both the scatter plots do not reveal any issue about the homogeneity of variance. Fig. 14c displays the histogram of residuals and Fig. 14d depicts the normal probability plot of residuals. It appears that the distribution of the residuals cannot be considered significantly different from the normal distribution, except for the extreme zones.
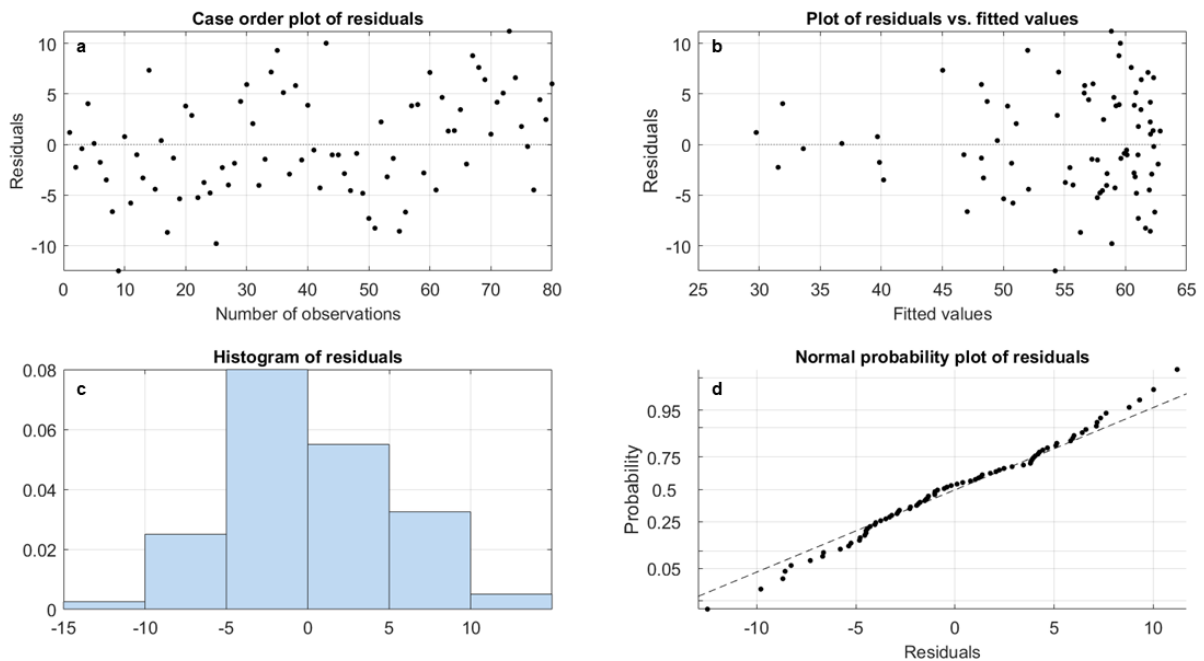
Fig. 14. Graphical residual analysis.

3.5 Predictive analysis

The purpose of the predictive analysis is to determine an algorithm that can predict accurately the electrode wear indicator through the electrode displacement signal. In PHM activity, Artificial Intelligence and Machine Learning algorithms are attracting a huge amount of interest both in industrial and academic fields [26]. The reason is the extraordinary predictive capabilities of such algorithms. Thus, a Machine Learning algorithm based on a Neural Network has been built to predict the wear indicator, the electrode contact area, by using all the selected features from the electrode displacement signal discussed earlier. Since the number of predictors and the number of observations used are quite limited, selecting a high number of neurons per layer and/or many layers would likely cause overfitting. For this reason, starting from a shallow Neural Network of one hidden layer and ten neurons, the optimal architecture was established by trial and error by changing both the number of neurons and the number of layers. The final NN architecture has involved two fully connected hidden layers and five neurons for each one. A sigmoid activation function has been used in hidden layers, whereas a linear activation function has been implemented for the output layer. A Bayesian regularization training function has been used to minimize the combination of the squared errors and weights, and to ensure good generalization properties in the test set. The dataset involves the inspected weld spots, split in 75% for the training set and 25% for the test set. The NN architecture is represented in Fig. 15.
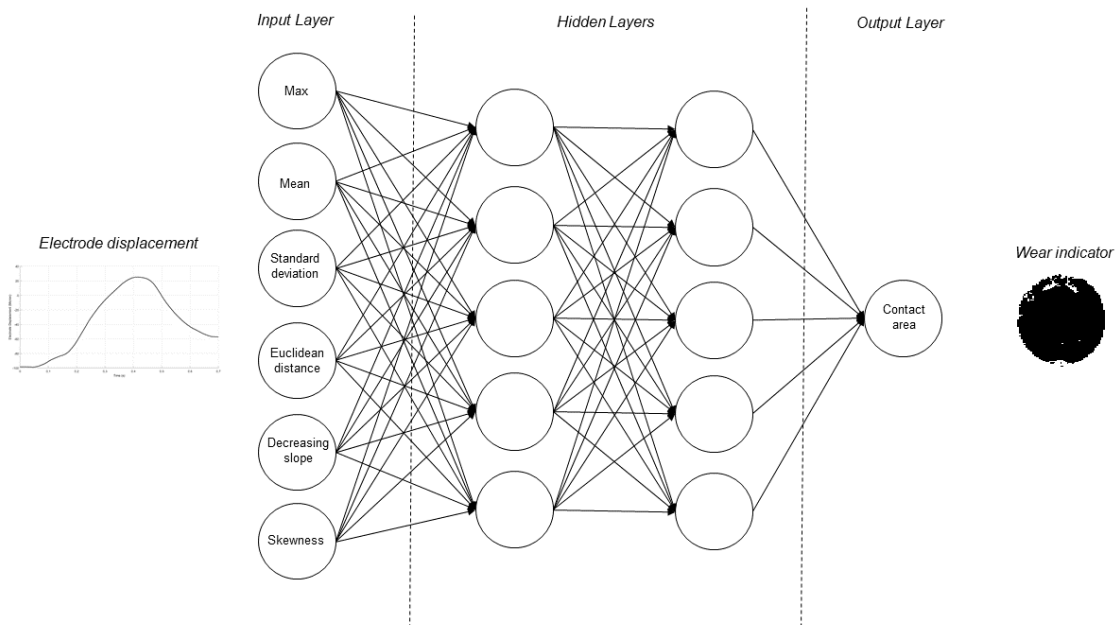
Fig. 15. Neural Network architecture.

The performances of the Neural Network are displayed in Fig. 16 and summarized in Table 3. The error has been evaluated as the difference between the observed value (i.e., electrode contact area) and predicted value, whereas the relative error has been computed as the ratio of the error and the observed value.
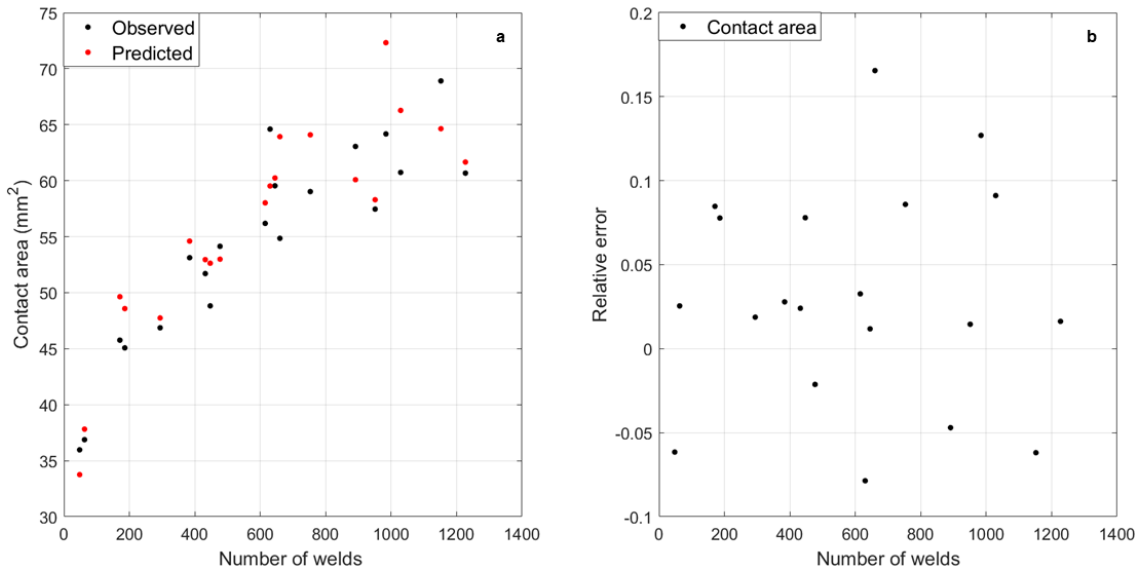
Fig. 16. Neural Network performances for the prediction of the electrode contact area and relative error.

Table 3
Neural Network performance metrics obtained from the data of Fig. 17a.

Mean error	Median error	Standard deviation	Mean relative error	Median relative error	Relative standard deviation
1.61 mm^2	1.11 mm^2	3.73 mm^2	0.03	0.02	0.06

Both the median error and the mean error are less than 2 mm^2, and the standard deviation is quite limited. The variability of the relative error, as estimated by its variance, is about 6 %, with both median value and mean value within 3 %. The scatter plot shows how the relative error is generally within 10 %.

The performances provided by Machine Learning algorithms allow more and more high predictive capabilities, allowing to predict in real-time the degradation of electrodes through welding signals and their replacement when the most significant geometrical feature, which characterizes the electrode wear, achieves a critical value. As a result, the electrodes could be replaced through the prediction of their contact areas based on the analysis of the electrode displacement during the welding process. A similar approach could be made more accurate, with an improvement of the predictive performance, through the integration of information from other physical sources, such as the electrical dynamic resistance, acquired by further sensors embedded in the RSW machine.

4. Conclusions

This work proposes a new method to indirectly monitor the electrode deterioration during resistance spot welding through the examination of electrode displacement, electrode face damage, as evaluated by a carbon imprint test, and mechanical strength of spot welds. A regression analysis has been set to find a relationship between the electrode face area, representative of tool degradation, and the electrode speed in the hold stage. A Neural Network has also been built to use some features extracted from the electrode displacement signals to predict the contact area and thus indirectly the electrode degradation.

The main achieved results are listed in the following.

- the contact area is the most suitable feature to describe the electrode degradation because of its ability to detect the loss of the mechanical strength of the joint during welding. Therefore, it can be considered as an appropriate indicator of electrode wear;

- the regression analysis has proved how the electrode speed during the hold stage is highly related to the contact area, explaining more than 70% of the contact area variation during the electrode deterioration process;
- based on some features from the electrode displacement signal, a Neural Network has been built to obtain an accurate prediction of the electrode contact area, and hence of electrode degradation, from features extracted from electrode displacement curves;
- the real time monitoring of the electrode displacement would allow predicting when to replace or dress the electrodes just before the achievement of critical wear conditions;
- this analysis can be a starting point towards the field of PHM activities of welding processes. A more accurate model for electrode life might be implemented to establish electrode life based on the computation of wear parameters through weld signal processing.

Future research will be focused on the exploration of a wider observation domain by carrying out experiments with different process parameters levels and by employing several types of sensors on the machine to improve the predictive capabilities of the ML algorithm.

Acknowledgments

References

[1]   S. Chen, T. Sun, X. Jiang, J. Qi, and R. Zeng, "Online monitoring and evaluation of the weld quality of resistance spot welded titanium alloy," *J. Manuf. Process.*, vol. 23, pp. 183–191, 2016, doi: 10.1016/j.jmapro.2016.06.003.

[2]   D. Zhao, Y. Bezgans, Y. Wang, W. Du, and D. Lodkov, "Performances of dimension reduction techniques for welding quality prediction based on the dynamic resistance signal," *J. Manuf. Process.*, vol. 58, no. July, pp. 335–343, 2020, doi: 10.1016/j.jmapro.2020.08.037.

[3]   D. Zhao, Y. Wang, D. Liang, and M. Ivanov, "Performances of regression model and artificial neural network in monitoring welding quality based on power signal," *J. Mater. Res. Technol.*, vol. 9, no. 2, pp. 1231–1240, 2020, doi: 10.1016/j.jmrt.2019.11.050.

[4]   X. Wan, Y. Wang, and D. Zhao, "Quality evaluation in small-scale resistance spot welding by electrode voltage recognition," *Sci. Technol. Weld. Join.*, vol. 21, no. 5, pp. 358–365, 2016, doi: 10.1080/13621718.2015.1115161.

[5]   X. Wan, Y. Wang, D. Zhao, Y. A. Huang, and Z. Yin, "Weld quality monitoring research in small scale resistance spot welding by dynamic resistance and neural network," *Meas. J. Int. Meas. Confed.*, vol. 99, pp. 120–127, 2017, doi: 10.1016/j.measurement.2016.12.010.

[6]   N. Haghshenas and H. Moshayedi, "Monitoring of Resistance Spot Welding Process," *Exp. Tech.*, vol. 44, no. 1, pp. 99–112, 2020, doi: 10.1007/s40799-019-00341-z.

[7]   Y. J. Xia *et al.*, "Online measurement of weld penetration in robotic resistance spot welding using electrode displacement signals," *Meas. J. Int. Meas. Confed.*, vol. 168, no. August 2020, p. 108397, 2021, doi: 10.1016/j.measurement.2020.108397.

[8]   Y. S. Zhang and G. L. Chen, "A neuro-fuzzy approach to part fitup fault control during resistance spot welding using servo gun," *Lect. Notes Comput. Sci.*, vol. 3612, no. PART III, pp. 1060–1068, 2005, doi: 10.1007/11539902_135.

[9]   Y. J. Xia, Z. W. Su, Y. B. Li, L. Zhou, and Y. Shen, "Online quantitative evaluation of expulsion in resistance spot welding," *J. Manuf. Process.*, vol. 46, no. June, pp. 34–43, 2019, doi: 10.1016/j.jmapro.2019.08.004.

[10] L. Zhou *et al.*, "Comparative study on resistance and displacement based adaptive output tracking control strategies for resistance spot welding," *J. Manuf. Process.*, no. December 2019, 2020, doi: 10.1016/j.jmapro.2020.03.061.

[11] D. Zhao, M. Ivanov, Y. Wang, D. Liang, and W. Du, "Multi-objective optimization of the resistance spot welding process using a hybrid approach," *J. Intell. Manuf.*, 2020, doi: 10.1007/s10845-020-01638-2.

[12] A. S. Kiselev and M. S. Slobodyan, "Effects of electrode degradation on properties of small-scale resistance spot welded joints of e110 alloy," *Mater. Sci. Forum*, vol. 970, no. September, pp. 227–235, 2019, doi: 10.4028/www.scientific.net/MSF.970.227.

[13] K. Mahmud, S. P. Murugan, Y. Cho, C. Ji, D. Nam, and Y. Do Park, "Geometrical degradation of electrode and liquid metal embrittlement cracking in resistance spot welding," *J. Manuf. Process.*, vol. 61, no. July 2020, pp. 334–348, 2021, doi: 10.1016/j.jmapro.2020.11.025.

[14] X. Q. Zhang, G. L. Chen, and Y. S. Zhang, "Characteristics of electrode wear in resistance spot welding dual-phase steels," *Mater. Des.*, vol. 29, no. 1, pp. 279–283, 2008, doi: 10.1016/j.matdes.2006.10.025.

[15] L. Zhou *et al.*, "Online monitoring of resistance spot welding electrode wear state based on dynamic resistance," *J. Intell. Manuf.*, no. 2016, 2020, doi: 10.1007/s10845-020-01650-6.

[16] Y. S. Zhang, H. Wang, G. L. Chen, and X. Q. Zhang, "Monitoring and intelligent control of electrode wear based on a measured electrode displacement curve in resistance spot welding," *Meas. Sci. Technol.*, vol. 18, no. 3, pp. 867–876, 2007, doi: 10.1088/0957-0233/18/3/040.

[17] H. Wang, Y. Zhang, and G. Chen, "Resistance spot welding processing monitoring based on electrode displacement curve using moving range chart," *Meas. J. Int. Meas. Confed.*, vol. 42, no. 7, pp. 1032–1038, 2009, doi: 10.1016/j.measurement.2009.03.005.

[18] J. Lee, J. Ni, J. Singh, B. Jiang, M. Azamfar, and J. Feng, "Intelligent Maintenance Systems and Predictive Manufacturing," *J. Manuf. Sci. Eng. Trans. ASME*, vol. 142, no. 11, 2020, doi: 10.1115/1.4047856.

[19] J. Peng, S. Fukumoto, L. Brown, and N. Zhou, "Image analysis of electrode degradation in resistance spot welding of aluminium," *Sci. Technol. Weld. Join.*, vol. 9, no. 4, pp. 331–336, 2004, doi: 10.1179/136217104225012256.

[20] I. Lum, S. Fukumoto, E. Biro, D. R. Boomer, and Y. Zhou, "Electrode Pitting in Resistance Spot Welding of Aluminum Alloy 5182," *Metall. Mater. Trans. A Phys. Metall. Mater. Sci.*, vol. 35 A, no. 1, pp. 217–226, 2004, doi: 10.1007/s11661-004-0122-8.

[21] S. Fukumoto, I. Lum, E. Biro, D. R. Boomer, and Y. Zhou, "Effects of electrode degradation on electrode life in resistance spot welding of aluminum alloy 5182," *Weld. J. (Miami, Fla)*, vol. 82, no. 11, 2003.

[22] B. Xing, Y. Xiao, and Q. H. Qin, "Characteristics of shunting effect in resistance spot welding in mild steel based on electrode displacement," *Meas. J. Int. Meas. Confed.*, vol. 115, no. June 2017, pp. 233–242, 2018, doi: 10.1016/j.measurement.2017.10.049.

[23] Y. J. Xia *et al.*, "Online measurement of weld penetration in robotic resistance spot welding using electrode displacement signals," *Meas. J. Int. Meas. Confed.*, vol. 168, no. September 2020, p. 108397, 2021, doi: 10.1016/j.measurement.2020.108397.

[24] Y. Ma, P. Wu, C. Xuan, Y. Zhang, and H. Su, "Review on techniques for on-line monitoring of resistance spot welding process," *Adv. Mater. Sci. Eng.*, vol. 2013, 2013, doi: 10.1155/2013/630984.

[25] P. Russo Spena, M. De Maddis, G. D'Antonio, and F. Lombardi, "Weldability and monitoring of resistance spot welding of Q&P and TRIP steels," *Metals (Basel).*, vol. 6, no. 11, 2016, doi: 10.3390/met6110270.

[26] L. Biggio and I. Kastanis, "Prognostics and Health Management of Industrial Assets: Current Progress and Road Ahead," *Front. Artif. Intell.*, vol. 3, no. November, pp. 1–24, 2020, doi: 10.3389/frai.2020.578613.